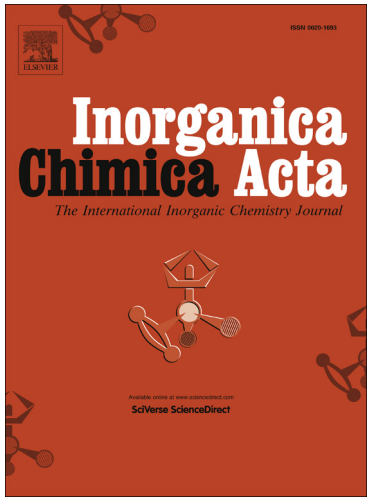

Synthesis, characterization, DFT calculations and biological activity of derivatives of 3-acetylpyridine and the zinc(II) complex with the condensation product of 3-acetylpyridine and semicarbazide

Božidar Čobeljić, Andrej Pevec, Iztok Turel, Marcel Swart, Dragana Mitić, Marina Milenković, Ivanka Marković, Maja Jovanović, Dušan Sladić, Marko Jeremić, Katarina Anđelković

PII: S0020-1693(13)00207-7
DOI: http://dx.doi.org/10.1016/j.ica.2013.04.017
Reference: ICA 15422

To appear in: *Inorganica Chimica Acta*

Received Date: 5 February 2013
Revised Date: 10 April 2013
Accepted Date: 11 April 2013

Please cite this article as: B. Čobeljić, A. Pevec, I. Turel, M. Swart, D. Mitić, M. Milenković, I. Marković, M. Jovanović, D. Sladić, M. Jeremić, K. Anđelković, Synthesis, characterization, DFT calculations and biological activity of derivatives of 3-acetylpyridine and the zinc(II) complex with the condensation product of 3-acetylpyridine and semicarbazide, *Inorganica Chimica Acta* (2013), doi: http://dx.doi.org/10.1016/j.ica.2013.04.017

Synthesis, characterization, DFT calculations and biological activity of derivatives of 3-acetylpyridine and the zinc(II) complex with the condensation product of 3-acetylpyridine and semicarbazide

Božidar Čobeljić[a], Andrej Pevec[b], Iztok Turel[b], Marcel Swart[c,d], Dragana Mitić[a], Marina Milenković[e], Ivanka Marković[f], Maja Jovanović[f], Dušan Sladić[a], Marko Jeremić[a], Katarina Anđelković[*a]

[a] *Faculty of Chemistry, University of Belgrade, Studentski trg 12-16, 11000 Belgrade, Serbia*

[b] *Faculty of Chemistry and Chemical Technology, University of Ljubljana, Aškerčeva 5, 1000 Ljubljana, Slovenia*

[c] *Institució Catalana de Recerca i Estudis Avançats (ICREA), Pg. Lluís Companys 23, 08010 Barcelona, Spain*

[d] *Institut de Química Computacional and Departament de Química, Universitat de Girona, Campus Montilivi, 17071 Girona, Spain*

[e] *Department of Microbiology and Immunology, Faculty of Pharmacy, University of Belgrade, Vojvode Stepe 450, Serbia*

[f] *Institute of Medical and Clinical Biochemistry, Faculty of Medicine, University of Belgrade, Pasterova 2, 11000 Belgrade, Serbia*

Keywords: Zn(II) complex, Schiff base, DFT calculations, biological activity

Abstract

A Schiff base of 3-acetylpyridine with semicarbazide as well as the corresponding tetrahedral Zn(II) complex were synthesized and characterized by X-ray crystal structure analysis and spectroscopic methods. It is interesting to note that the ligand coordinated as a monodentate although there are several donor atoms in it. Computational studies showed that such structure is more stable than the hypothetical structure with one ligand bound as a bidentate. The complex exibited moderate antibacterial, antifungal and cytotoxic activities while the ligand was mostly inactive. The complex strongly induced formation of reactive

oxygen species in tumor cell lines. It also influenced cell cycle progression in tumor cell lines, and induced autophagy. The latter effect is, at least in part, a protective one.

1. Introduction

Condensation derivatives of 2-acetylpyridine with hydrazines, hydrazides and dihydrazides and their transition metal compexes have been extensively studied by our group [1–3]. These ligands have a large number of possible donor atoms and therefore display a diverse behavior in metal coordination. The central metal atom and the nature of the ligand determine the way of coordination.

There is a small number of papers concerning derivates of 3-acetylpyridine and their complexes in none of which biological activity was studied [4–8]. Bis hydrazone of hydrazine and 3-acetylpyridine was coordinated to Zn(II) via pyridine nitrogen and not via hydrazone nitrogen [4].

In the complexes of Pt(II), Co(II), Ni(II) and Cu(I) with condensation derivative of 3-acetylpyridine and thiosemicarbazide the ligand is coordinated as a bidentate via thione sulfur and azomethine nitrogen while the heteroaromatic nitrogen is not involved in coordination [5–7].

There is only one publication concerning complexes of the condensation derivative of 3-acetylpyridine with semicarbazide. Based on similarity of spectral properties of oxovanadium(IV) complexes with 3-acetylpyridine semicarbazone and 2-acetylpyridine semicarbazone and X-ray structure of the latter complex, it was assumed that the 3-acetylpyridine derivative was coordinated as a monodentate in neutral form via the carbonyl oxygen of the side chain [8].

Zinc is considered the most abundant trace intracellular element and a substantial amount of this element is incorporated in the nucleus [9]. As some other metal ions zinc has many positive physiological effects but changes in its metabolism or trafficking may be related to some diseases [10,11].

Zinc(II) ions are present in zinc finger proteins that recognize and bind to DNA [12,13]. In zinc fingers the zinc ion is usually tetrahedrally coordinated by cysteine and histidine residues [14]. Lippert has stressed that the role of zinc in nucleic acid chemistry is unique in many aspects [15]. For example, from all metal ions only zinc(II) ions are able to facilitate the rewinding of molten DNA [15].

In the present paper condensation products of 3-acetylpyridine with different hydrazide type compounds were studied for their coordination behavior and antitumor and antimicrobial activities. The present work describes synthesis, characterization and biological activity of derivatives of 3-acetylpyridine with semicarbazide, oxamic hydrazide, ethyl carbazate and

zinc(II) complex with 3-acetylpyridine semicarbazone. Coordination behaviour of the ligands was investigated by DFT calculations.

2. Experimental

2.1. Materials and methods

All solvents (reagent grade) were obtained from commercial suppliers and used without further purification. The elemental analyses (C, H, N) were performed by the standard micromethods using the ELEMENTAR Vario ELIII C,H,N analyser. IR spectra were recorded on Perkin-Elmer FT-IR 1725X spectrophotometer by the KBr technique in the region 4000–400 cm^{-1}. Abbreviations used for IR spectra: vs, very strong; s, strong; m, medium; w, weak. NMR spectral assignments and structural parameters were obtained by combined use of ^{1}H homonuclear spectroscopy (2D NOESY) and multinuclear proton-detected spectroscopy (2D HSQC, 2D HMBC). The NMR spectra were performed on Bruker Avance 500 equipped with broad-band direct probe. All spectra were measured at 298 K. 2D NOESY spectra were collected with 4 scans per t1-increment and mixing time of 1 s. Chemical shifts are given on δ scale relative to tetramethylsilane (TMS) as internal standard for ^{1}H and ^{13}C. Abbreviations used for NMR spectra: s, singlet; d, doublet; dd, doublet of doublets; t, triplet; q, quartet; m, multiplet. All microorganism tests were performed in Műller Hinton broth for the bacterial strains and in Sabouraud dextrose broth for the yeast. Human promyelocytic leukemia (HL-60), human glioma (U251), rat glioma (C6), mouse fibrosarcoma (L929) and mouse melanoma (B16) cell lines were obtained from the European Collection of Animal Cell Cultures (Salisbury, UK). Flow cytometry analysis was performed on a FACSCalibur flow cytometer (BD Biosciences, Heidelberg, Germany), using CellQuest Pro software for acquisition and analysis. All statistical data were analyzed by t-test or ANOVA followed by Student-Newman-Keuls test. Statistical significance of the differences of means was analyzed at the significance level of $p < 0.05$.

2.2. Synthesis of (2E)-2-[1-(pyridin-3-yl)ethylidene]hydrazinecarboxamide hydrochloride dihydrate (**HL1**, $C_8H_{15}ClN_4O_3$)

3-Acetylpyridine (0.11 cm^{-3}, 1 mmol) was added to a solution of semicarbazide hydrochloride (111 mg, 1 mmol) in water (25 cm^{-3}) and the mixture was refluxed for 3 h.

After 7 days colorless crystals were obtained (180 mg, 72%), mp 214–230 ºC. Anal. Calc. for $C_8H_{15}ClN_4O_3$: C, 38.33; H, 6.03; N, 22.35. Found: C, 38.53; H, 6.08; N, 22.49 %. ^{1}H NMR (500 MHz; DMSO-d_6; Me_4Si): δ = 9.84 (s, 1 H, N(3)H), 9.39 (d, 1 H, ^4J = 1.7, H-1), 8.96 (m, 1 H, ^3J = 8.9, ^4J = 1.8, H-5), 8.81 (dd, 1 H, ^3J = 6.3, ^4J = 0.8, H-3), 8.02 (dd, 1 H, ^3J = 8.2, ^4J = 2.8, H-4), 6.75 (s, 2 H, N(4)H_2), 2.26 (s, 3 H, C(7)H_3) ppm; ^{13}C NMR (125 MHz, DMSO-d_6; Me_4Si): δ = 156.90 (C-8), 141.72 (C-5), 140.32 (C-1), 139.43 (C-6), 138.73 (C-3), 137.28 (C-2), 126.64 (C-4), 12.92 (C-7) ppm. IR (KBr; ν/cm^{-1}): $\overline{\nu}$ = 3424vs, 3289vs, 2358w, 2167w, 1691s, 1573m, 1533m, 1455m, 1411m, 1313w, 1247w, 1157m, 1088w, 892w, 668m.

2.3. Synthesis of 2'-[1-(3-pyridinyl)ethylidene]oxamohydrazide (**HL2**, $C_9H_{10}N_4O_2$)

To a solution of oxamic hydrazide (103 mg, 1 mmol) in water (25 cm^{-3}) 3-acetylpyridine (0.11 cm^{-3}, 1 mmol) was added and the mixture was refluxed for 3 h. After 4–5 days colorless crystals were obtained (130 mg, 65%), m.p.: 240 ºC. Anal. Calc. for $C_9H_{10}N_4O_2$: C, 52.42; H, 4.89; N, 27.17. Found: C, 52.17; H, 4.86; N, 26.92 %.. ^{1}H NMR (500 MHz; DMSO-d_6; Me_4Si): δ = 10.88 (s, 1 H, N(3)H), 9.00 (d, 1 H, ^4J = 2.0, H-1), 8.65 (m, 1 H, ^3J = 6.0, ^4J = 1.5, H-5), 8.35 (s, 1 H, N(4)H_2), 8.22 (dd, 1 H, ^3J = 7.5, ^4J = 1.5, H-3), 8.05 (s, 1 H, N(4)H_2), 7.50 (dd, 1 H, ^3J = 5.5, ^5J = 3.0, H-4), 2.36 (s, 3 H, C(7)H_3) ppm. ^{13}C NMR (125 MHz, DMSO-d_6; Me_4Si): δ = 161.92 (C-9), 156.68 (C-8), 155.47 (C-6), 150.20 (C-5), 147.32 (C-1), 134.39 (C-3), 133.28 (C-2), 123.69 (C-4), 14.03 (C-7) ppm. IR (KBr; ν/cm^{-1}): $\overline{\nu}$ =: 3392m, 3268s, 3059vs, 2931m, 2651m, 2118w, 1725w, 1692vs, 1605s, 1511m, 1366s, 1175m, 974w, 816m, 646w

2.4. Synthesis of ethyl (2E)-2-[1-(pyridin-3-yl)ethylidene]hydrazinecarboxylate hydrochloride hydrate (**HL3**, $C_{10}H_{16}ClN_3O_3$)

To a solution of ethyl carbazate (104 mg, 1 mmol) in water (25 cm^{-3}) was added 3-acetylpyridine (0.11 cm^{-3}, 1 mmol) followed by a few drops of conc. HCl and the mixture was refluxed for 3 h. After 10 days colorless crystals were formed (200 mg, 76%), m.p.: 215 ºC. Anal. Calc. for $C_{10}H_{16}ClN_3O_3$: C, 45.89; H, 6.16; N, 16.06. Found: C, 45.73; H, 6.16; N, 15.87 %. ^{1}H NMR (500 MHz; DMSO-d_6; Me_4Si): δ = 10.59 (s, 1 H, N(3)H), 9.05 (d, 1 H, ^4J = 2.0, H-1), 8.87 (dd, 1 H, ^3J = 5.6, ^4J = 1.0, H-5), 8.77 (m, 1 H, ^3J = 8.5, ^4J = 1.5, H-3), 8.04 (dd, 1 H, ^3J = 6.0, ^5J = 2.0, H-4), 4.18 (q, 2 H, ^3J = 7.0 C(9)H_2), 2.30 (s, 3 H, C(7)H_3), 1.24 (s,

3 H, C(10)H_3) ppm. ^{13}C NMR (125 MHz, DMSO-d_6; Me_4Si): δ= 153.99 (C-8), 143.74 (C-6), 141.52 (C-5), 141.41 (C-1), 139.42 (C-3), 137.15 (C-2), 126.79 (C-4), 61.02 (C-9), 14.55 (C-7), 13.64 (C-10) ppm. IR (KBr; ν/cm^{-1}): $\overline{\nu}$ =: 3407s, 3361s, 2997vs, 2361w, 2026w, 1738vs, 1644m, 1550m, 1530s, 1462s, 1395m, 1229vs, 1041m, 890w, 727w.

2.5. Synthesis of the complex [$ZnCl_2(HL1)_2$] (**1**, $C_{16}H_{20}Cl_2N_8O_2Zn$)

To a solution containing (2*E*)-2-[1-(pyridin-3-yl)ethylidene]hydrazinecarboxamide hydrochloride (**HL1**) (25 mg, 0.1 mmol) in methanol (15 cm^{-3}) was added $Zn(CH_3COO)_2{\cdot}2H_2O$ (21 mg, 0.1 mmol) dissolved in 5 cm^{-3} of methanol. The mixture was refluxed for 4 h forming a colorless solution. After ten days white crystals suitable for X-ray diffraction were formed (18 mg, 73 %), m.p.: 240 ºC. Anal. Calc. for $C_{16}H_{20}Cl_2N_8O_2Zn$: C, 39.01; H, 4.09; N, 22.74. Found: C, 38.91; H, 4.15; N, 22.44 %. ^{1}H NMR (500 MHz; DMSO-d_6; Me_4Si): δ= 9.17 (s, 2 H, N(3)H), 8.96 (s, 2 H, H-1), 8.55 (d, 2 H, ^3J = 7.5, H-5), 8.08 (d, 2 H, ^3J = 7.8, H-3), 7.36 (dd, 2 H, ^1J = 7.8, ^3J = 5.0, H-4), 6.25 (s, 4 H, N(4)H_2), 2.27 (s, 6 H, C(7)H_3) ppm. ^{13}C NMR (125 MHz, DMSO-d_6; Me_4Si): δ = 157.29 (C-8), 148.84 (C-5), 146.91 (C-1), 141.63 (C-6), 134.09 (C-3), 133.67 (C-2), 123.70 (C-4), 13.10 (C-7) ppm. IR (KBr; ν/cm^{-1}): $\overline{\nu}$ =: 3430m, 3196m, 1697s, 1630w, 1466m, 1314w, 1098m, 1058m, 824w, 768w, 695w, 537w.

2.6. *Crystal structure determination*

Crystal data and refinement parameters of compounds **HL1**, **HL3** and **1** are listed in Table S1. The X-ray intensity data were collected at room temperature with a Nonius Kappa CCD diffractometer equipped with graphite-monochromated Mo Kα radiation (λ = 0.71073 Å) for **HL1** and **1** and with an Agilent SuperNova dual source with an Atlas detector equipped with mirror-monochromated Mo Kα radiation (λ = 0.71073 Å). The data were processed by using DENZO [16] or *CrysAlis* PRO [17]. The structures were solved by direct methods (SHELXS-97 [18] for **HL1** and **1** and SIR-92 [19] for **HL3**) and refined by a full-matrix least-squares procedure based on F^2 using SHELXL-97 [18]. All non-hydrogen atoms were refined anisotropically. All hydrogen atoms bonded to carbon were included in the model at geometrically calculated positions and refined using a riding model. The N-bound hydrogen atoms were located in a difference map and refined with the distance

restraints (DFIX) with N-H = 0.86 and with U_{iso}(H) = 1.2U_{eq}(N). The water hydrogen atoms in **HL1** and **HL3** were located in a difference map and refined using distance restraints (DFIX) with O–H = 0.96 and with U_{iso}(H) = 1.2U_{eq}(O).

2.7. Microorganisms

The antimicrobial activity was evaluated using seven different laboratory control strains of bacteria, i.e., the Gram-positive: *Staphylococcus aureus* (ATCC 25923), *Staphylococcus epidermidis* (ATCC 12228), *Kocuria rhizophila* (ATCC 9341), *Bacillus subtilis* (ATCC 6633) and the Gram-negative: *Escherichia coli* (ATCC 25922), *Klebsiella pneumoniae* (ATCC 13883), *Pseudomonas aeruginosa* (ATCC 27853), and two strains of yeast, i.e., *Candida albicans* (ATCC 10259 and ATCC 10231). Overnight broth cultures of each strain were prepared, and the final concentration in each well was adjusted to 2 x 10^6 CFU mL^{-1} for the bacteria and 2 x 10^5 CFU mL^{-1} for the yeast. The investigated compounds were dissolved in 1% dimethyl sulfoxide (DMSO) and then diluted to the highest concentration. Two-fold serial concentrations of the compounds were prepared in a 96-well microtiter plate over the concentration range 31.25–500 μg mL^{-1}. The microbial growth was determined after 24 h incubation at 37 ºC for the bacteria and after 48 h incubation at 26 ºC for the fungi. The MIC is defined as the lowest concentration of the compound at which no visible growth of microorganism is observed.

2.8. Brine shrimp assay

A teaspoon of lyophilized eggs of the brine shrimp *Artemia salina* was added to 1 L of the artificial sea water containing several drops of yeast suspension (3 mg of dry yeast in 5 mL distilled water), and air was passed through the suspension thermostated at 28 ºC, under illumination for 24 h. The tested substances were dissolved in DMSO. In a glass vial, into 1 mL of artificial sea water 1–2 drops of yeast extract solution (3 mg in 5 mL of distilled water) and 10–20 hatched nauplii were added, and finally solutions of all derivatives to the appropriate concentrations. For each concentration, two determinations were performed. The vials were left at 28 ºC under illumination for 24 h, and afterwards live and dead nauplii were counted. LC50 was defined as the concentration of a drug that causes death of 50% nauplii. DMSO was inactive under applied conditions.

2.9. Cells and treatment

Human promyelocytic leukemia (HL-60), human glioma (U251), rat glioma (C6), mouse fibrosarcoma (L929) and mouse melanoma (B16) cell lines were obtained from the European Collection of Animal Cell Cultures (Salisbury, UK). The cells were cultured at 37 °C in a humidified atmosphere with 5% CO_2, in a HEPES (20 mM)-buffered RPMI 1640 cell culture medium supplemented with 2 mM L-glutamine, antibiotic/antimycotic mixture (1%) and 5% of fetal bovine serum (FBS) (all from PAA, Pasching, Austria). For the cell viability assessment, the cells were incubated in 96-well flat-bottom plates (2×10^4 cells/well). For the flow cytometric analysis, the cells were incubated in 24-well plates (2×10^5 cells/well). Cells were rested for 24 h and then treated with the complex, its corresponding ligand or cisplatin. Stock solutions of ligand and complex were made in water, and of cisplatin in DMSO. In experiments with cisplatin, both the untreated control cells and an additional control cell culture containing the appropriate amount of DMSO (always less than 0.5%) were investigated and no significant difference was observed (data not shown).

2.10. Cell number determination

The acid phosphatase assay was used to measure cell numbers as previously described [20]. The assay is based on the hydrolysis of the *p*-nitrophenyl phosphate by intracellular acid phosphatases in viable cells to produce *p*-nitrophenol. In brief, *p*-nitrophenyl phosphate solution (10 mM *p*-nitrophenyl phosphate in 0.1 M sodium acetate buffer, pH 5.5, with 0.1% Triton X-100) was added to each well and the samples were incubated for 2 hours. Reaction was stopped by addition of NaOH (1 M) and the absorbance, which is directly proportional to the cell number, was measured in an automated microplate reader at 405 nm (Sunrise, TECAN, UK). The results were presented as % absorbance relative to untreated control cultures. The IC_{50} values were calculated using GraphPad Prism (GraphPad Software Inc.).

2.11. Flow cytometric analysis of apoptotic parameters, ROS production and acidic vesicle detection

Flow cytometry analysis was performed on a FACSCalibur flow cytometer (BD Biosciences, Heidelberg, Germany), using CellQuest Pro software for acquisition and analysis. Cell cycle parameters were assessed by flow cytometric analysis of ethanol-fixed

cells stained with DNA-binding dye propidium iodide (PI) as previously described [20]. The results are presented as a percentage (%) of cells in different phases of cell cycle (G_0/G_1, S, G_2/M), and in sub-G_0 compartment (hypodiploid cells), that were considered apoptotic. Intracellular production of reactive oxygen species was determined by measuring the intensity of green fluorescence (FL1) emitted by the redox-sensitive dye dihydrorhodamine 123 (DHR; Sigma-Aldrich, St. Louis, MO), which was added to cell cultures (1 μM) at the beginning of treatment. The content of acidic vesicles (i.e. lysosomes, autolysosomes) was quantified by flow cytometry following supravital acridine orange staining. After incubation, cells were washed with PBS and stained with acridine orange (1 μM; Sigma, St. Louis, MO) for 15 min at 37 ^{o}C. Accumulation of acidic vesicles was quantified as red/green fluorescence ratio (mean FL3/FL1), and the results presented as representative histograms with mean ± SD values from three separate experiments.

2.12. Computational details

All of the density functional calculations were carried out with the Amsterdam Density Functional (ADF, version 2012.01) [21,22] program. Uncontracted basis sets of Slater-type orbitals (STOs) of triple-ζ quality plus polarization functions (TZP, using the frozen-core approach [22]) and even-tempered basis sets of quadruple-ζ quality (ET-pVQZ) [23] were used. The geometries were obtained at the PBE-D/TZP [24,25] level, and energies and NMR chemical shifts were obtained at SSB-D/ET-pVQZ [26]. Both functionals include Grimme's dispersion (D_2) corrections [25]. All calculations included a dielectric continuum solvation model (COSMO [27–29]), with parameters appropriate for water (geometries) or DMSO (NMR). The geometry optimizations were carried out with the QUILD program [30] that uses superior optimization routines based on adapted delocalized coordinates [31]. The NMR chemical shifts were referenced against tetramethylsilane (TMS). The SSB-D functional was recently found to be one of the best density functionals for obtaining computed NMR chemical shifts [32].

3. Results and discussion

3.1. General

The condensation reaction of 3-acetylpyridine and semicarbazide, oxamic hydrazide and ethyl carbazate in water was performed similary to the procedure by Wyrzykiewicz and Blaszczyk [33], affording three ligands: **HL1**, **HL2** and **HL3** (Scheme 1), respectively. Using these ligands and $Zn(OAc)_2 \cdot 2H_2O$ in molar ratio 2:1 in methanol solution only in the case of **HL1** a defined product could be isolated. Zn(II) complex with the formula $[ZnCl_2(HL1)_2]$ (**1**) was obtained with two ligands **HL1** coordinated in a monodentate fashion (Scheme 1).

Scheme 1.

3.2. Description of the crystal structures

To confirm the coordination of **HL1** to Zn cation single-crystal X-ray analysis was undertaken. The molecular structure of complex **1** is shown in Fig. 1. Crystal structures and hydrogen-bonding representation of compounds **HL1** and **HL3** are illustrated in Figures S1–S4 in the Supplementary material. Crystal data, structure refinement defects and the selected bond distances and bond angles of **HL1**, **HL3** and **1** are listed in Tables S1 and S2. Hydrogen bonding geometry of compounds **HL1**, **HL3** and **1** are given in Table S3. Compound **1** cystallizes in orthorhombic crystal system (space group *Pbcn*) where the Zn(II) ions are lying on a two-fold rotation axes. The geometry around the metal centre is tetrahedral. The two **HL1** ligands are monodentately coordinated through the pyridine N1 atom with Zn–N1 distance of 2.055(2) Å. The Zn–Cl bond distance in complex **1** is 2.2298(6) Å. The average of the Zn containing angles is 110.7º and this is very close to ideal tetrahedron angle. In the compound **1** there are two N–H···O hydrogen bonding interactions including hydrazine N3 and amide N4 atom as a donor and carbonyl oxygen O1 as an acceptor. These interactions lead to the formation of 2D puckered layer in the crystal structure (Fig. 2).

Fig. 1.

Fig. 2.

3.3. NMR studies

Comparison of ^{1}H NMR spectra of the complex **1** with those of **HL1** ligand gave additional support for the structure. It was observed that all protons of the free ligand were observed in the spectrum of the complex, suggesting that no deprotonation occurred. In the spectrum of the complex large upfield shifts of pyridine ring atoms were observed upon complexation, suggesting that coordination occurred via pyridine nitrogen.

Further confirmation was established by comparing the ^{13}C NMR spectrum of the free ligand with that of the complex, indicating that the ligand was coordinated as a monodentate, since there were large changes in chemical shifts of pyridine ring carbons, and small changes of side chain carbon signals.

Complexes with ligands **HL2** and **HL3** could not be isolated. Therefore, NMR spectra in DMSO-d_6 solution of mixtures of $Zn(CH_3COO)_2{\cdot}2H_2O$ and either **HL1**, **HL2** or **HL3** (mole ratio metal : ligand = 1 : 2) were recorded. the ligands differed in their behaviour. In case of **HL1** only sharp signals of the complex were detected. In case of **HL3** two sets of signals for all the pyridine hydrogens were observed, with approximate ratio free ligand : bound ligand = 3 : 2. In case of **HL2** signals of the ligand were shifted and broadened, indicating an equilibrium between free and complexed ligand. No changes in signal positions for the surroundings oh the other possible donor atoms were observed, so that in all cases only pyridine nitrogen was coordinated.

3.4. Computational studies

The structure of **1** was corroborated by a computational study at the PBE-D/TZP level [24,25], including solvent effects through a dielectric continuum model (COSMO) [27–29]. Two structures were obtained with an energy difference (at SSB-D [26] / ET-pVQZ [23]) of ca. 0.3 kcal·mol^{-1}. The only difference between them is the rotation of the **HL1** ligands as a whole as shown in Fig. 3. As can be seen from this figure, it hardly has an effect on the Zn–ligand distances. The computed distances are very close to the X-ray distances (Zn–N 2.07 Å, Zn–Cl 2.27 Å).

Fig. 3.

We also computed the NMR data at the SSB-D/ET-pVQZ level, which has recently been [32] found to be one of the best methods to predict ^{1}H and ^{13}C chemical shifts. The

computed shifts agree well with the experimental spectra (see Supplementary material, Table S4), and support the formation of compound **1**. The formation of **1** with two **HL1** ligands in monodentate coordination, and not the formation of a compound with only **HL1** ligand in a bidentate coordination, is further corroborated by the computed reaction energies (at SSB-D/ET-pVQZ):

$1 \cdot \mathbf{HL1} + ZnCl_2 \rightarrow ZnCl_2(HL1)_1$ $\Delta E = -28.4$ kcal·mol^{-1}

$2 \cdot \mathbf{HL1} + ZnCl_2 \rightarrow ZnCl_2(HL1)_2$ (**1**) $\Delta E = -43.8$ kcal·mol^{-1}

Futhermore, binding energies for the formation a complex with **HL2** ligand (–40.2 kcal/mol) and **HL3** ligand (–40.9 kcal/mol) at the same level of theory, indicate that the other two zinc complexes are also possible and would have similar structures but up to now we were unable to isolate them. The experimental NMR evidence shows that complexes with **HL2** and **HL3** are less stable which is in accordance with calculated binding energies.

3.5. Antimicrobial activity

The complex **1** exhibited moderate antimicrobial activity. All tested strains of microorganisms were sensitive. The best inhibitory effect was detected against *Staphylococcus epidermidis, Kocuria rhizophila, Bacillus subtilis* and *Pseudomonas aeruginosa* (MIC values 62.5 μg /ml). Inhibitory activity against all other tested bacteria was significantly lower (MIC values >100 μg/mL). Interestingly, one strain of yeast *Candida albicans* (ATCC 10259), was more sensitive than the other one (Table 1). The ligand **HL1** as well as compounds **HL2**, **HL3** and zinc acetate were inactive.

Table 1

Antimicrobial activity.

Microorganism	**HL1 (μg/mL) (MIC)**	**HL2 (μg/mL) (MIC)**	**HL3 (μg/mL) (MIC)**	**1 (μg/mL) MIC**	**$Zn(OAc)_2 \cdot 2H_2O$ (μg/mL) MIC**
Staphylococcus aureus ATCC 25923	>500	>500	250.0	125.0	>500
Staphylococcus epidermidis ATCC 12228	>500	>500	500.0	62.5	500

Kocuria rhizophila ATCC 9341	>500	>500	500.0	62.5	250
Bacillus subtilis ATCC 6633	>500	>500	500.0	62.5	500
Escherichia coli ATCC 25922	>500	>500	>500	125.0	>500
Klebsiella pneumoniae ATCC 13883	>500	>500	>500	125.0	>500
Pseudomonas aeruginosa ATCC 27853	>500	>500	>500	62.5	>500
Candida albicans ATCC 10259	>500	>500	500	62.5	500
Candida albicans ATCC 10231	>500	>500	500	125.0	500

3.5. *Brine shrimp test*

In the brine shrimp test which can be correlated to cell-line toxicity and antitumor activity [34,35] **1** showed a moderate activity (Table 2), the ligand being less active. In this test compounds **HL2** and **HL3** showed a weak to moderate activity.

Table 2

Toxic effect (expressed as LC_{50} values in μM) of the investigated compounds on *Artemia salina*.

Compound	**LC_{50} (μM)**
HL1	0.395
HL2	0.371
HL3	0.684
1	0.205
$Zn(OAc)_2 \cdot 2H_2O$	0.674

3.6. Antitumor activity

The acid phosphatase assay demonstrated that the investigated complex reduced the cell numbers in cultures of the five tested cancer cell lines in a dose-dependent manner, while the ligand was inactive (Table 3.).

Table 3

The cytotoxicity of ligand and complex in various cancer cell lines and comparison with cisplatin.

	IC_{50} (μM)				
compound	**B16**	**C6**	**L929**	**HL-60**	**U251**
cisplatin	42.15 ± 1.52	12.9 ± 4.8	11.2 ± 3.4	1.50 ±0.09	14.5 ± 3.3
HL1	>100	>100	>100	>100	>100
1	91.01 ± 3.58	92.96 ± 5.21	41.70 ± 3.62	63.54 ± 5.14	80.91 ± 4.72

We next assessed if overproduction of reactive oxygen species (ROS) could be responsible for the observed cytotoxic effects of **1**. Complex **1** strongly induced the formation of ROS in both HL-60 and L929 cell lines, reaching the peak after 6 hours of incubation, as measured by DHR fluorescence (Fig. 4a–c). However, this was not accompanied by rise in superoxide (O_2^-) production, since, after the same incubation times, no increase in superoxide-derived dihydroethidium (DHE) fluorescence was observed (data not shown). It may therefore be assumed that the observed increase in ROS production cannot be attributed to the superoxide overproduction induced by **1**, but rather to decrease in the antioxidative capacity of the cells. Contrary to **1**, ligand **HL1** showed no activity.

The role of ROS in cytotoxic effect of **1** was further confirmed by pretreatment with ROS scavenger, *N*-acetylcysteine (NAC). NAC pretreatment partially abolished the cytotoxic action of **1**. (Fig. 4d). These data indicate that the antitumor effect of **1** at least in part depends on ROS.

Fig. 4.

In order to further explore the observed antitumor effects of **1**, its ability to influence the cell cycle progression was tested. The propidium iodide-based analysis of the DNA content in HL-60 leukemic (Fig. 5a and c) and L929 fibrosarcoma cells (Fig. 5b and d) revealed that complex **1** at the concentration of 100 μM (48 h) induced DNA fragmentation in both cell

lines (17.34% and 20.55% of cells in sub G_0 phase, respectively), together with decrease in proliferation rate, indicated by the reduced percentage of cells in S and G_2/M phase. The slowing down in the DNA replication was especially pronounced in HL-60 cell line, where percentage of cell in S phase decreased from 33.95% (Fig. 5a), to 21.38% (Fig. 5c).

Fig. 5.

It has been shown that high level of ROS can induce autophagy, a catabolic process involving the degradation of the cell's own components and damaged molecules in autolysosomes [36]. The ability of **1** to induce autophagy in the HL-60 leukemia (Fig. 6a and c) and L929 mouse fibrosarcoma cell line (Fig. 6b and d) was next assessed. Flow cytometry analysis of acridine orange-stained cells demonstrated a clear increase in red/green (FL3/FL1) fluorescence ratio in both HL-60 (Fig. 6c) and L929 cells (Fig. 6d) exposed to **1** (100 μM, 24h), compared to the untreated, control cells (Fig. 6a and b). This indicated that treatment with **1** caused intracellular accumulation of acidic organelles (lysosomes/autolysosomes), that is consistent with autophagy induction. In order to establish the role of autophagy in the observed cytotoxic effect of **1**, i.e. if observed autophagy induction contributes to cell death, or has a protective role, cell viability of L929 cells was measured in the presence of potent proton pump inhibitor bafilomycin A1, that impairs lysosomal acidification. Bafilomycin treatment, in concentration that alone did not affect cell viability (100 nM) caused further decrease in cell viability (from 42.9% to 30.2%), indicating that autophagy induction may, at least in part, help diminish the cytotoxic effect of **1** on L929 cell line.

Fig. 6.

4. Conclusion

A Zn(II) complex of the Schiff base of 3-acetylpyridine and semicarbazide, where two ligands were monodentately coordinated, was obtained. This behaviour is a consequence of a much higher stability of the structure of the complex with two ligands bound as monodentates than the hypothetical structure with one ligand bound as a bidentate, as calculated at SSB-D/ET-pVQZ level of theory.

Complex **1** showed moderate antibacterial, antifungal and cytotoxic activities. It is likely that the biological activity is a consequence of overproduction of ROS. The complex **1** induced autophagy in tumor cell lines, which is a protective effect from cytotoxic action of **1**.

Abbreviations

HL1	(2*E*)-2-[1-(pyridin-3-yl)ethylidene]hydrazinecarboxamide hydrochloride dihydrate
HL2	2'-[1-(3-pyridinyl)ethylidene]oxamohydrazide
HL3	(2*E*)-2-[1-(pyridin-3-yl)ethylidene]hydrazinecarboxylate hydrochloride hydrate
TMS	tetramethylsilane
COSY	correlation spectroscop
HSQC	Heteronuclear Single Quantum Coherence
HMBC	Heteronuclear Multiple Bond Correlation
HL-60	Human promyelocytic leukemia
U251	human glioma
C6	rat glioma
L929	mouse fibrosarcoma
B16	mouse melanoma
PI	propidium iodide
ROS	reactive oxygen species

Acknowledgment

This work was supported by the Ministry of Education and Science of the Republic of Serbia (Grant OI 172055 and III41025). We thank the Slovenian Research Agency (ARRS) thrugh program P-0175 for financial support and EN-FIST Centre of Excellence, Dunajska 156, 1000 Ljubljana, Slovenia, for using SuperNova diffractometer. The following organizations are thanked for financial support: the Ministerio de Ciencia e Innovación (MICINN, project number CTQ2011-25086/BQU), and the DIUE of the Generalitat de Catalunya (project number 2009SGR528). Financial support from MICINN (Ministry of Science and Innovation, Spain) and the FEDER fund (European Fund for Regional Development) was provided by grant UNGI08-4E-003. Excellent service by the Centre de Serveis Científics i Acadèmics de Catalunya (CESCA) is gratefully acknowledged.

Appendix A. Supplementary data

Crystallographic data for the ligands HL1 and HL3 and the complex $[ZnCl_2(HL1)_2]$ may be obtained from the Cambridge Crystallographic Data Centre (CCDC, 12 Union Road, Cambridge CB2 1EZ, UK; fax: (+44) 1223-336-033; e-mail: deposit@ccdc.cam.ac.uk or www: http://www.ccdc.cam.ac.uk) on quoting the depository numbers CCDC 901497, 901498 and 901499, respectively.

Supplementary data to this article can be found online at doi...

References

[1] K. Anđelković, J. Howing, R. Tellgren, D. Jeremić, I. Ivanović-Burmazović, D. Sladić, J. Coord. Chem. 56 (2003) 611–622.

[2] A. Bacchi, G. Pelizzi, D. Jeremić, M. Gruden-Pavlović, K. Anđelković, Transition Met. Chem. 28 (2003) 935–938.

[3] R. Eshkourfu, B. Čobeljić, M. Vujčić, I. Turel, A. Pevec, K. Sepčić, M. Zec, S. Radulović, T. Srdić-Radić, D. Mitić, K. Andjelković, D. Sladić, J. Inorg. Biochem. 105 (2011) 1196–1203.

[4] M. Khanpour, A. Morsali, CrystEngComm 11 (2009) 2585–2587.

[5] I.C. Mendes, L.R. Teixeira, R. Lima, T.G. Carneiro, H. Beraldo, Transition Met. Chem. 24 (1999) 655–658.

[6] H. Beraldo, W.F. Nacif, L.R. Teixeira, J.S. Reboucas, Transition Met. Chem. 27 (2002) 85–88.

[7] R.L. de Lima, L.R. Teixeira, T.M.Gomes Carneiro, H. Beraldo, J. Braz. Chem. Soc. 10 (1999) 184–188.

[8] A. Mena, B. Bastos, J.G. da Silva, P.I. da S. Maia, V.M. Deflon, A.A. Batista, A.V.M. Ferreira, L.M. Botion, E. Niquet, H. Beraldo, Polyhedron, 27 (2008) 1787–1794.

[9] R.J. Cousins, Proc. Nutr. Soc. 57 (1998) 307–311.

[10] L.A. Finney, T.V. O'Halloran, Science 300 (2003) 931–936.

[11] I. Turel, J. Kljun, Curr. Top. Med. Chem. 11 (2011) 2661–2687.

[12] N.P. Pavletich, C.O. Pabo, Science 252 (1991) 809–817.

[13] J.W.R. Schwabe, D. Rhodes, Trends Biochem. Sci. 16 (1991) 291–299.

[14] D. Voet, Biochemistry, John Wiley & Sons, Inc. Hoboken, 2004.

[15] E.C. Fusch, B. Lippert, J. Am. Chem. Soc. 116 (1994) 7204–7209.

[16] Z. Otwinowski, W. Minor, Methods Enzymol. 276 (1970) 307–326.

[17] Oxford Diffraction (2009). CrysAlis PRO. Oxford Diffraction LTD. Yarnton, England.

[18] G.M. Sheldrick, Acta Crystallogr. A 64 (2008) 112–122.

[19] A. Altomare, G. Cascarano, C. Giacovazzo, A. Guagliardi, J. Appl. Crystallogr. 26 (1993) 343–350.

[20] T.T. Yang, P. Sinai, S.R. Kain, Anal. Biochem. 241 (1996) 103–108.

[21] Baerends ADF 2012.01

[22] G. te Velde, F.M. Bickelhaupt, E.J. Baerends, C. Fonseca Guerra, S.J.A. van Gisbergen, J.G. Snijders, T. Ziegler, J. Comput. Chem. 22 (2001) 931–967.

[23] D.P. Chong, E. van Lenthe, S. van Gisbergen, E.J. Baerends, J. Comput. Chem. 25 (2004) 1030–1036.

[24] J.P. Perdew, K. Burke, M. Ernzerhof, Phys. Rev. Lett. 77 (1996) 3865–3868.

[25] S. Grimme, J. Comput. Chem. 27 (2006) 1787–1799.

[26] M. Swart, M. Sola, F.M. Bickelhaupt, J. Chem. Phys. 131 (2009) 094103-1–094103-9.

[27] A. Klamt, G. Schuurmann, J. Chem. Soc. Perkin Trans. II 2 (1993) 799–805.

[28] C.C. Pye, T. Ziegler, Theor. Chem. Acc. 101 (1999) 396–408.

[29] M. Swart, E. Rosler, F.M. Bickelhaupt, Eur. J. Inorg. Chem. 2007 (2007) 3646–3654.

[30] M. Swart, F.M. Bickelhaupt, J. Comput. Chem. 29 (2008) 724–734.

[31] M. Swart, F.M. Bickelhaupt, Int. J. Quantum Chem. 106 (2006) 2536–2544.

[32] L. Armangué, M. Sola, M. Swart, J. Phys. Chem. A 115 (2011) 1250–1256.

[33] E. Wyrzykiewicz, A. Blaszczyk, J. Heterocyclic Chem. 37 (2000) 975–981.

[34] B.N. Meyer, N.R. Ferrigni, J.E. Putnam, L.B. Jacobsen, D.E. Nichols, J.L. McLaughlin, Planta Med. 45 (1982) 31–34.

[35] J.E. Anderson, C.M. Goetz, J.L. McLaughlin, M. Suffness, Phytochem. Anal. 2 (1991) 107–111.

[36] Lj. Harhaji, A. Isakovic, N. Raicevic, Z. Markovic, B. Todorovic-Markovic, N. Nikolic, Sanja Vranjes-Djuric, Ivanka Markovic, Vladimir Trajkovic, Eur J Pharmacol. 568 (2007) 89–98.

Figure captions:

Fig. 1. Molecular structure of **1**, showing the atom-numbering scheme.

Fig. 2. Hydrogen-bonding network of compound **1**.

Fig. 3. Two conformations of **1**, related to each other by a rotation of the **HL1** ligands as a whole. The compound in red is almost identical to the X-ray structure (see Fig. 1).

Fig. 4. Induction of oxidative stress by **1.** (a) HL-60 and (b) L929 cells were incubated with **1** for 6 hours, stained with dihydrorhodamine 123 and analyzed by flow cytometry. (c) Time-dependence of the increase in ROS production. (d) The cell viability of L929 cells following the treatment with **1** (100 μM) for 48 hours, in conditions of pretreatment (1 hour) with ROS scavanger, *N*-acetylcysteine (NAC) assessed by acid phosphatase assay. Flow cytometry histograms of DHR-stained L929 and HL-60 cells from the representative of 3 separate experiments are presented. ($*p < 0.05$).

Fig. 5. The effects of **1** on cell cycle and apoptosis of tumor cells. L929 and HL-60 cells were cultivated for 48 h in the absence or presence of 100 μM **1**, stained with propidium iodide (PI) following fixation in ethanol. DNA content/cell cycle analysis was performed by flow cytometry in the control (HL-60, a; L929, b) and treated cells (HL-60, c; L929, d). The histograms from the representative experiment are presented, while cell cycle distribution values are means from three independent experiments.

Fig. 6. Induction of autophagy by **1.** L929 and HL-60 cells were cultivated for 24h in the absence or presence of 100 μM **1**, stained with acridine-orange and autophagy induction was examined by flow cytometry. The treatment caused increase in red/green (FL3/FL1) fluorescence ratio in both (c) HL-60 and (d) L929 cells exposed to **1** (100 μM, 24h), compared to the respective control cells (a and b). The results are presented as representative histograms and FL3/FL1 ratio presented as mean±SD from three independent experiments.

Scheme Caption:

Scheme 1. Synthesis of the ligands **HL1**, **HL2**, **HL3** (a) and the formation of complex $[ZnCl_2(HL1)_2]$ (**1**) (b).

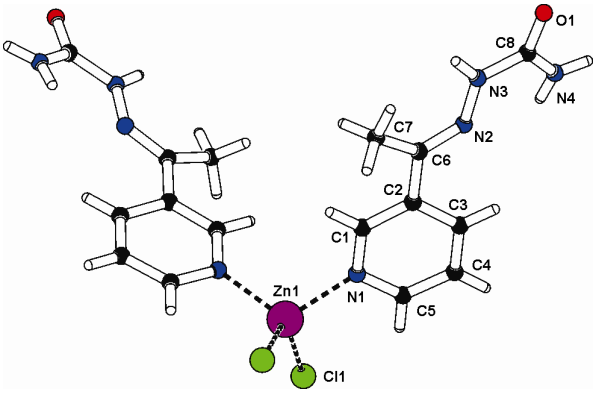

Fig. 1.

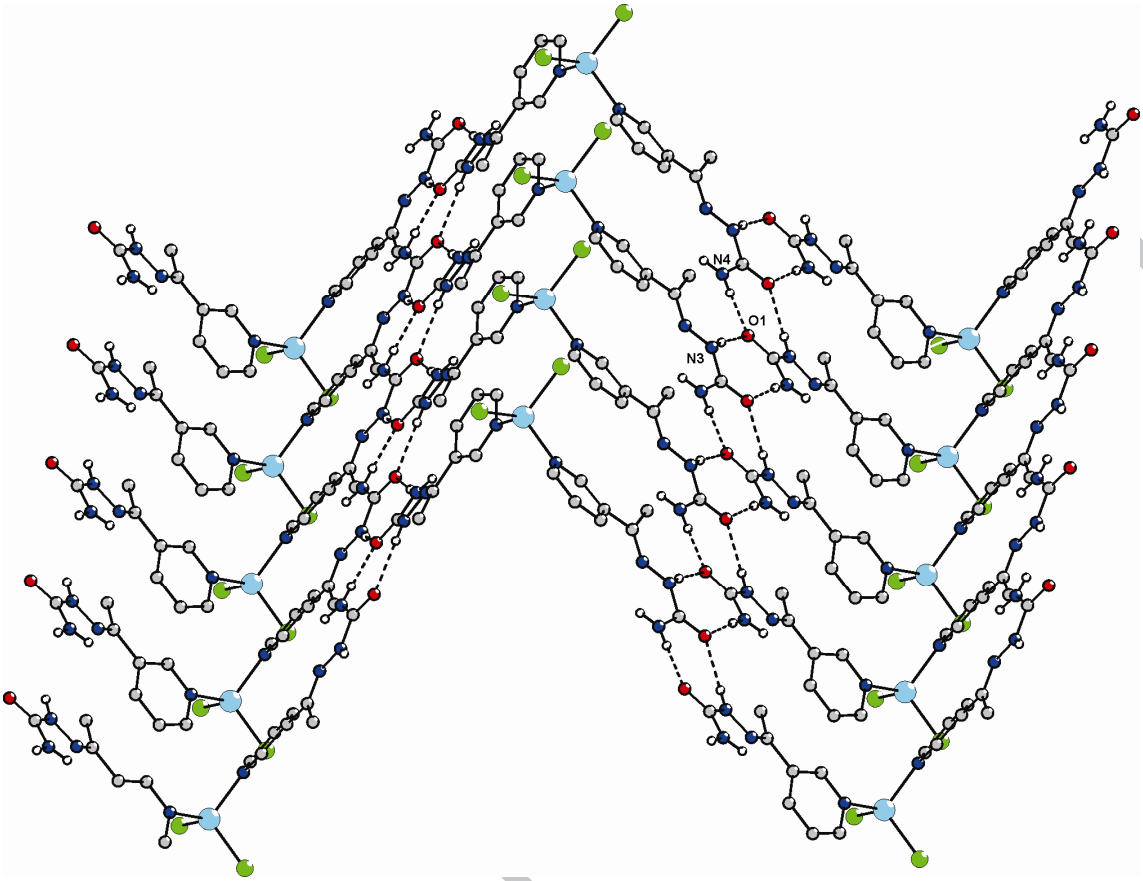

Fig. 2.

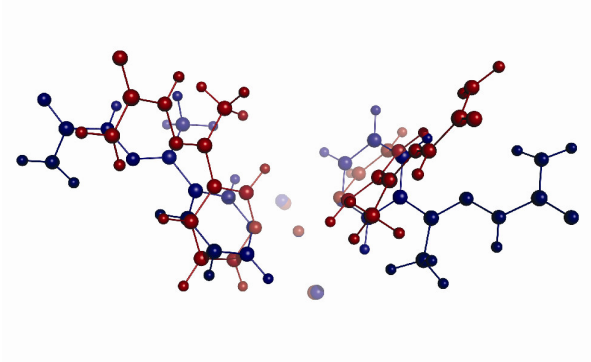

Fig. 3.

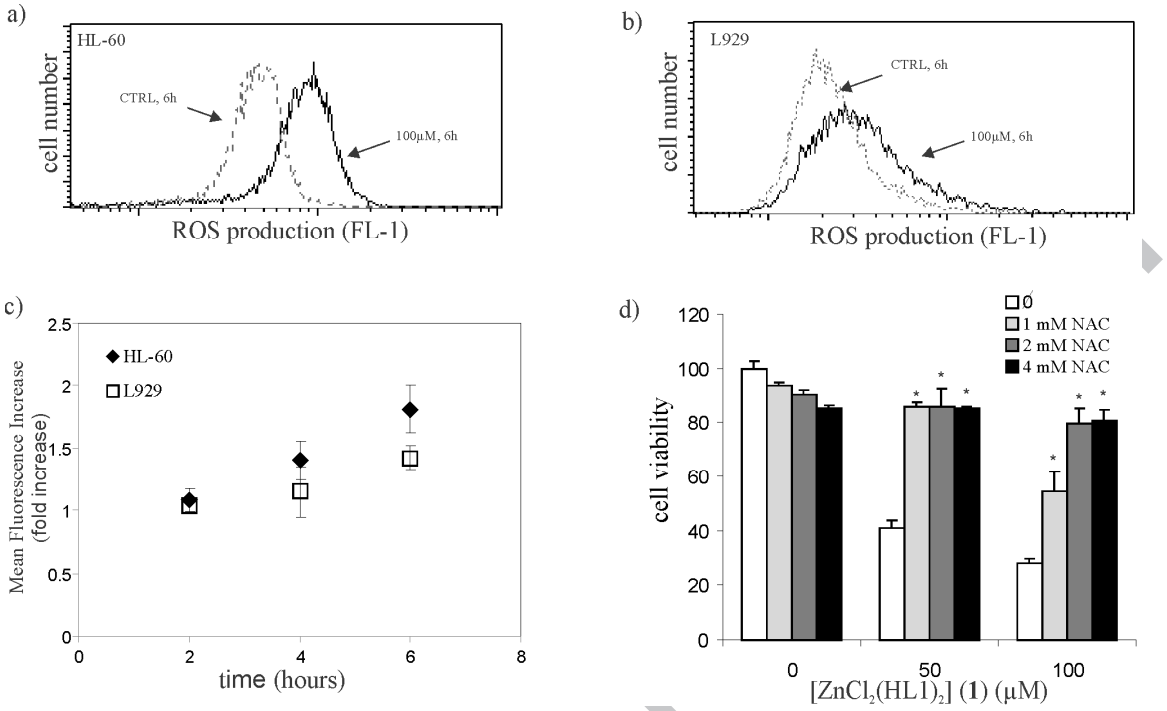

Fig. 4.

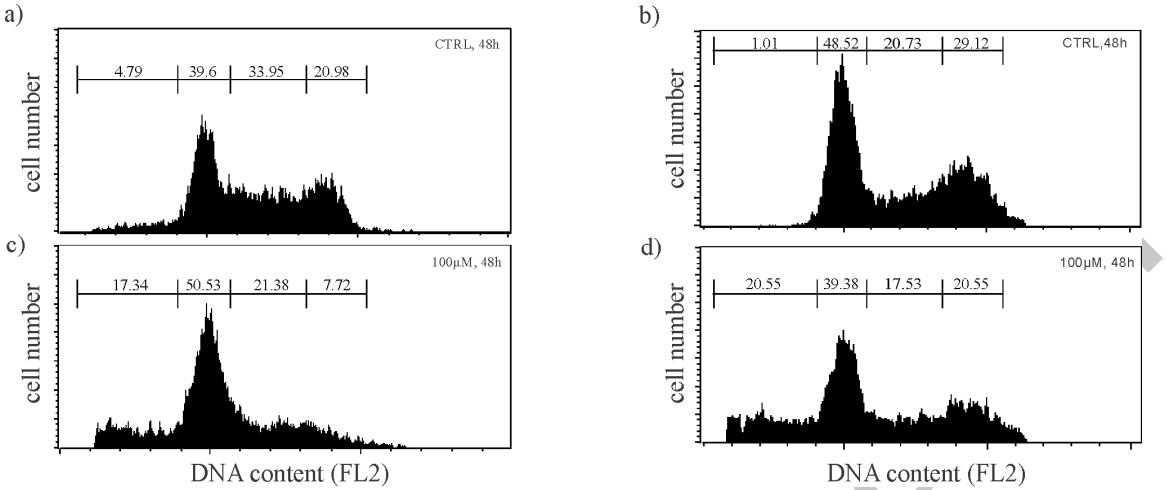

Fig. 5.

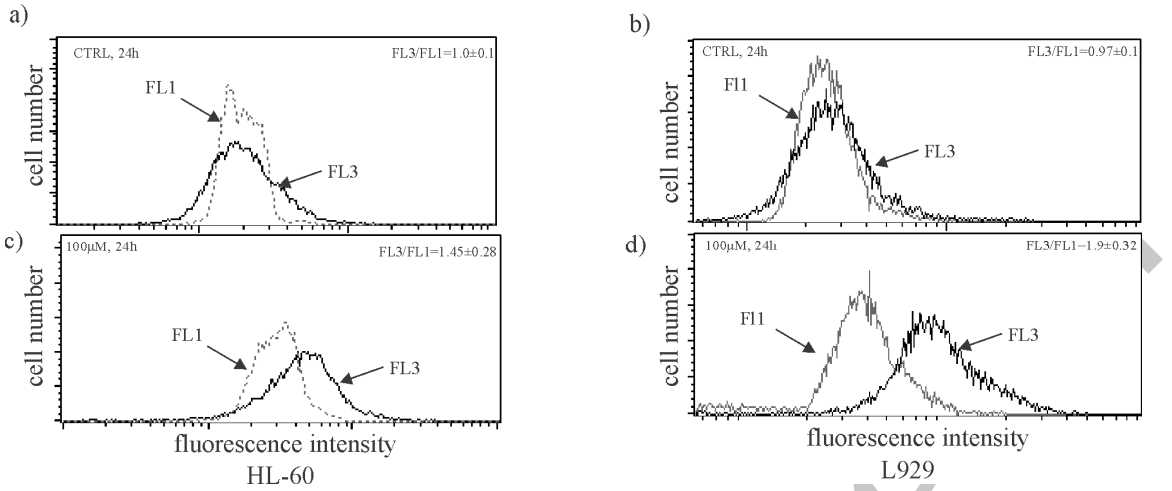

Fig. 6.

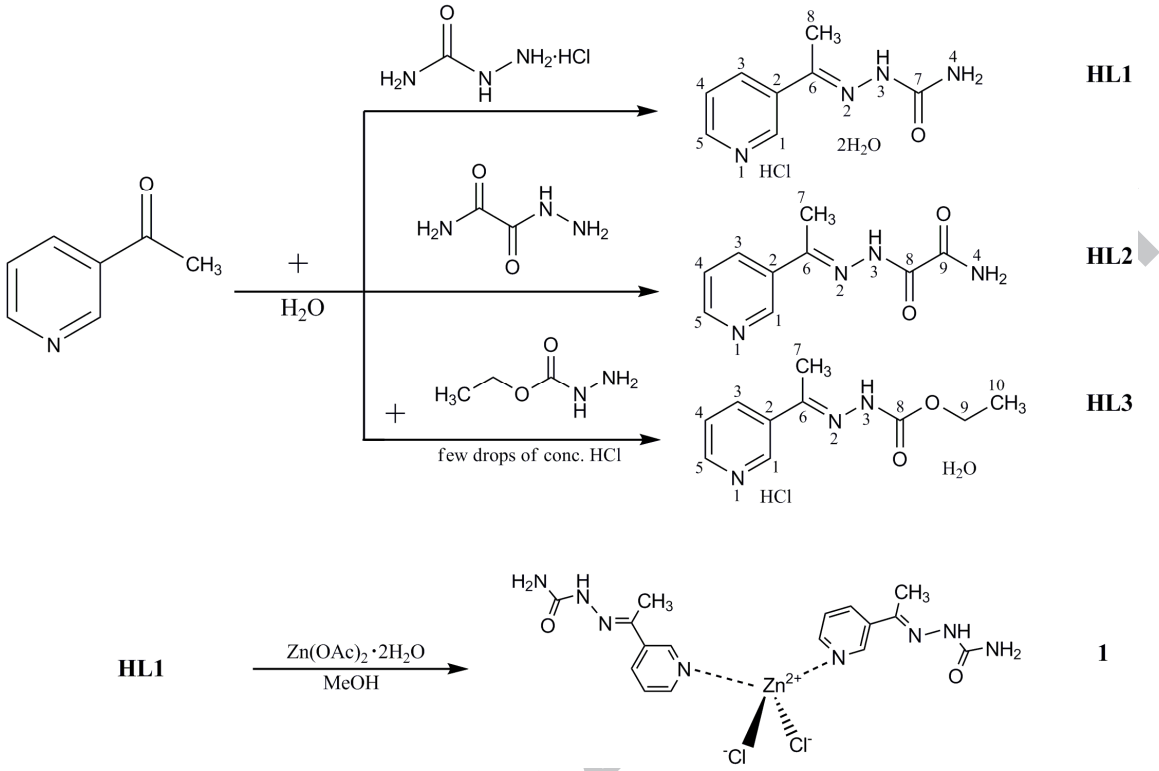

Scheme 1.

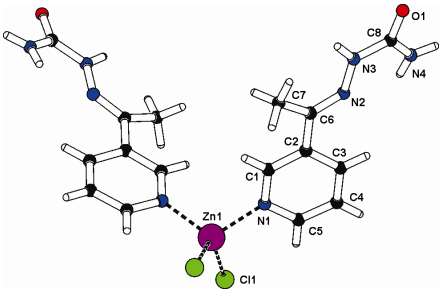

- Tetrahedral complex of Zn(II) with 3-acetylpyridine semicarbazone
- DFT calculations on stabilities of various structures
- Moderate antibacterial, antifungal and cytotoxic activities
- Induction of ROS in tumor cell lines by a complex with a non-redox active metal
- Effect on cell cycle progresion in tumor cell lines and induction of autophagy